

A Search for Star Formation in the Smith Cloud

David V. Stark^{1*}, Ashley D. Baker¹, Sheila J. Kannappan¹

¹*Physics and Astronomy Department, University of North Carolina, Chapel Hill, NC 27516*

Accepted 2014 October 16. Received 2014 October 16; in original form 2014 June 20

ABSTRACT

Motivated by the idea that a subset of HVCs trace dark matter substructure in the Local Group, we search for signs of star formation in the Smith Cloud, a nearby $\sim 2 \times 10^6 M_\odot$ HVC currently falling into the Milky Way. Using *GALEX* NUV and *WISE*/2MASS NIR photometry, we apply a series of color and apparent magnitude cuts to isolate candidate O and B stars that are plausibly associated with the Smith Cloud. We find an excess of stars along the line of sight to the cloud, but not at a statistically significant level relative to a control region. The number of stars found in projection on the cloud after removing an estimate of the contamination by the Milky Way implies an average star formation rate surface density of $10^{-4.8 \pm 0.3} M_\odot \text{ yr}^{-1} \text{ kpc}^{-2}$, assuming the cloud has been forming stars at a constant rate since its first passage through the Milky Way ~ 70 Myr ago. This value is consistent with the star formation rate expected based on the average gas density of the cloud. We also discuss how the newly discovered star forming galaxy Leo P has very similar properties to the Smith Cloud, but its young stellar population would not have been detected at a statistically significant level using our method. Thus, we cannot yet rule out the idea that the Smith Cloud is really a dwarf galaxy.

Key words: Galaxies: ISM: clouds — galaxies: star formation – ISM: Individual Objects: Smith Cloud

1 INTRODUCTION

Since the discovery of high velocity clouds (HVCs), astronomers have explored a variety of scenarios to explain their nature and origin (see Wakker & van Woerden 1997 and references therein). As a possible solution to the ‘missing satellites problem’ (e.g., Klypin et al. 1999), both Blitz et al. (1999) and Braun & Burton (1999) proposed that HVCs, or the subset of compact HVCs (CHVCs), trace low mass dark matter halos in the Local Group. Sternberg et al. (2002) argue against CHVCs being embedded in halos at typical distances of ~ 1 Mpc because their dark matter halos would have unrealistic densities, although they find that CHVCs are consistent with being embedded in dark matter minihalos that are circumgalactic with distances of ~ 150 kpc. More recently, a new class of HVCs, called ultra-compact HVCs (UCHVCs), was discovered in the ALFALFA survey and have properties consistent with being dark matter halos spread throughout the Local Group (Giovanelli et al. 2010; Adams et al. 2013).

If all or a subset of HVCs trace dark matter substructure around the Milky Way, they might contain some (potentially very faint) stellar population. In contrast, in the absence of dark matter, such star formation may

never occur. Based on calculations without dark matter, Christodoulou et al. (1997) argue that the dense cores in high velocity clouds never reach high enough mass to collapse on their own, and the cloud-cloud collision timescale for these cores within a single complex is > 1 Gyr. However, simulations of infalling HVCs without dark matter imply they survive less than ~ 100 Myr before they are dispersed (Heitsch & Putman 2009; Nichols & Bland-Hawthorn 2009; Joung et al. 2012).

Aside from considerations about dark matter content, star formation in HVCs faces additional challenges. The average observed HI column density in HVCs is roughly $\sim 10^{19} \text{ cm}^{-2}$ (Putman et al. 2012), whereas star formation (at least in galaxy disks) is typically associated with HI column densities above 10^{21} cm^{-2} (e.g., de Blok & Walter 2006). Molecular gas, which is considered direct fuel for star formation, has only been successfully detected in a handful of HVCs (Richter et al. 2001; Sembach et al. 2001; Hernandez et al. 2013). In addition, HVCs have very low metallicity (10–30% solar) and dust content. No HVCs, with the exception of the Magellanic Stream, show depletion of refractory elements, and dust has only been tentatively detected from FIR emission in a handful of cases (Putman et al. 2012). Low dust content may be an important factor when considering star formation since H_2 formation is catalyzed by dust grains (Gould & Salpeter 1963). However, alternative viewpoints

* dstark@email.unc.edu

say that the formation of H_2 in itself is not the cause of star formation but simply a process that also occurs in dense gas (Mac Low & Glover 2012), so the existence of dust in itself may not be crucial. The recent discovery of star formation in low gas density, low metallicity XUV disks (Thilker et al. 2007) calls into question many presumptions about the conditions in which star formation can occur.

There have been multiple attempts to search for stellar populations in high velocity clouds. An extensive search of POSS imaging by Simon & Blitz (2002) found no associated stellar populations in a sample of 250 northern sky HVCs, suggesting that HVCs are not associated with normal but faint dwarf galaxies like those already found in the Local Group. Several smaller studies have focused on identifying overdensities of red giant or blue luminous stars at the positions of high-latitude and often compact HVCs, and these studies have likewise found no associated stellar populations (Willman et al. 2002; Hopp et al. 2003; Siegel et al. 2005; Hopp et al. 2007). Based on their own search for stellar populations associated with HVCs in combination with those of other groups up to that point, Hopp et al. (2007) argued that no more than 4 per cent of HVCs could harbor star formation.

On the other hand, some searches for stellar populations associated with HVCs have proven fruitful. A single YSO in close proximity to a high-velocity HI emission peak was identified by Ivezić & Christodoulou (1997), who argued that the probability of such an occurrence being observed due to a random projection is extremely low. More recently, McQuinn et al. (2013) and Rhode et al. (2013) reported on a stellar population associated with Leo P, an object originally classified as an ultra compact HVC (UCHVC) after its discovery in the ALFALFA survey (Giovanelli et al. 2013).

In this study, we search for signs of star formation in Complex GCP, commonly known as the Smith Cloud (Smith 1963), in an attempt to constrain the likelihood that it hosts a dark matter halo. The Smith Cloud is a nearby low latitude HVC with total neutral and ionized hydrogen mass $> 2 \times 10^6 M_\odot$ (Lockman et al. 2008; Hill et al. 2009). There are several advantages to studying the Smith Cloud. It has a peak column density of $\sim 5 \times 10^{20} \text{ cm}^{-2}$, putting it in a low gas density regime that still hosts star formation as seen by Bigiel et al. (2008), although we note that the Smith Cloud is dynamically very different from the extended galactic HI disks in that work. While the low latitude of the Smith Cloud has the practical disadvantage of higher foreground extinction, its ongoing interaction with the Milky Way may trigger star formation (as in, e.g., Casetti-Dinescu et al. 2014).

The fact that the Smith Cloud has survived as long as it has is additional evidence that it is embedded within a dark matter halo. Extrapolation of its trajectory implies it must have already passed through the Milky Way disk ~ 70 Myr ago and is on track to collide with the disk again in another ~ 30 Myr (Lockman et al. 2008). Nichols et al. (2014) argue it could never have survived its passage through the Galactic disk without dark matter, although the recent detection of magnetic fields by Hill et al. (2013) provides an additional means to contain the cloud. A final advantage of studying the Smith Cloud is that it is one of the few HVCs with a well determined distance based on multiple techniques (Bland-Hawthorn et al. 1998; Putman et al. 2003; Lockman et al. 2008; Wakker et al. 2008), allowing an

additional means to isolate stars that could be associated with the cloud. Detection of a stellar population associated with the Smith Cloud could suggest that some HVCs are indeed associated with dark matter halos/subhalos, and perhaps only HVCs with such halos are capable of star formation.

In this work, we use a combination of *GALEX* NUV and 2MASS/*WISE* NIR photometry to search for evidence of recent star formation in the Smith Cloud. To accomplish this goal, we apply a series of color and magnitude cuts to isolate young stars consistent with being associated with the Smith Cloud. While we find a slight overdensity of young stars in projection in the region of the Smith Cloud, this overdensity is not statistically significant compared to the density of a control region. However, our estimate of the star formation rate is consistent with what would be expected based on the observed gas density. We cannot rule out the possibility that the Smith Cloud hosts low level star formation, and our analysis suggests that the recently discovered stellar population in Leo P, whose global properties are similar to the Smith Cloud, would not have been detected at a statistically significant level by our methods.

2 DATA AND METHODS

Below we describe our sources of data. All reported magnitudes are corrected for foreground extinction using the dust maps of Schlegel et al. (1998) and the extinction law of O'Donnell (1994).

2.1 21cm Data

This study uses GBT 21cm observations of the Smith Cloud presented in Lockman et al. (2008). To separate Smith Cloud emission from foreground Milky Way emission, a zero-moment map was created using all channels corresponding to $V_{LSR}=75-125 \text{ km s}^{-1}$. For our analysis, we need to define what is considered to be ‘on’ versus ‘off’ the cloud. The outermost $N_{\text{HI}} = 5 \times 10^{19} \text{ cm}^{-2}$ contour traces the overall head-tail structure of the cloud (see Fig. 1), so we refer to all regions within it as ‘on’ the cloud, while regions beyond it are considered ‘off’ the cloud. In § 3.2, we address how our results are affected by this definition.

2.2 Photometric Data

2.2.1 *GALEX*

Deep *GALEX* NUV imaging was obtained for 7 fields in the vicinity of the Smith Cloud (program GI6-041, PI Stark), with most fields covering regions on or around the cometary head where the densest gas is located. Each field covers a circular diameter of 1.2° and integration times vary from 1800–4697 seconds. Due to the failure of the FUV channel on *GALEX* prior to our observing program, no FUV imaging is available for these same regions. Additional All-sky Imaging Survey (AIS) data have been used to enlarge the NUV coverage beyond the border of the cloud. While the AIS images only have typical exposure times of ~ 100 seconds, they are still deep enough to detect young OB stars at the distance of the Smith Cloud (see § 2.3.3). In total, the

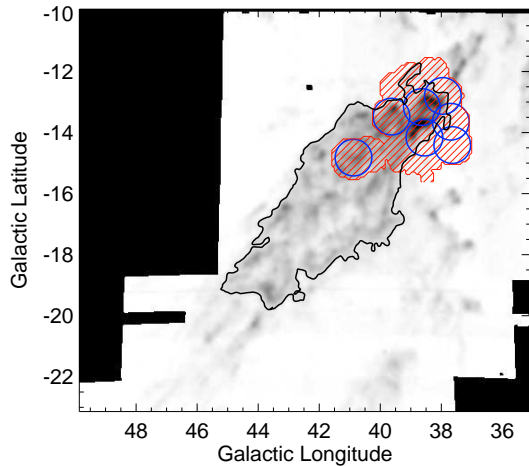


Figure 1. HI column density map of the Smith Cloud, adapted from Lockman et al. (2008). Square black regions represent masked pixels in the data cube. The thick black line shows the outermost $N_{\text{HI}} = 5 \times 10^{19} \text{ cm}^{-2}$ contour used to define the edge of the cloud. The red filled region illustrates the extent of the *GALEX* data used in this study, with the positions of deeper *GALEX* fields overlaid in blue.

Table 1. Control Region Fields

Field	l°	b°
1	317.49	-12.22
2	320.25	-14.91
3	326.01	-14.25

GALEX coverage extends over 11.04 deg^2 , with 6.08 deg^2 and 4.96 deg^2 lying ‘on’ and ‘off’ the cloud, respectively, using the definitions from § 2.1.

In addition, we acquired archival data for three Medium Imaging Survey (MIS) depth fields (totaling 3.39 deg^2) at comparable Galactic latitude but opposite Galactic longitude to the Smith Cloud. We use these as control regions far from the Smith Cloud but roughly equidistant from the Galactic bulge and mid-plane. The central coordinates of these three fields are given in Table 1.

All data products used in this study result from the standard *GALEX* imaging pipeline (Morrissey et al. 2007).

2.2.2 WISE & 2MASS

We have taken *WISE* $3.6\mu\text{m}$ and $4.5\mu\text{m}$ photometry¹ from the *WISE* All-Sky Source Catalog (Wright et al. 2010). After rejecting extended/blended objects and sources contaminated by artifacts, the *GALEX* and *WISE* data are cross-matched using a $3''$ match radius. Approximately 45 per cent of the *GALEX* sources lack detected *WISE* counterparts;

¹ We explored the use of *W3* and *W4* imaging to look for heated dust emission in the Smith Cloud that would be characteristic of young stars. However, the IR emission from the foreground Milky Way dominates the field. Disentangling the two emission sources is not trivial, so we did not pursue this further.

the majority of these sources have extremely low signal-to-noise (<3) and lie near the sensitivity limit of the *GALEX* data. We ignore these in our subsequent analysis since they are inconsistent with being OB stars at the distance of the Smith Cloud (see § 2.3.3).

We also use 2MASS *JHK* photometry, which has already been crossmatched with *WISE* sources and included in the *WISE* All-Sky Source Catalog. Because 2MASS data are shallower than *WISE* data, a small fraction of *GALEX* objects with corresponding *WISE* data lack 2MASS counterparts. Therefore, *GALEX* and *WISE* photometry are used in our primary analysis, with 2MASS being incorporated when available.

In the Smith Cloud fields (including regions both on and off the cloud), there are a total of 41,783 objects with measured *GALEX* NUV and *WISE* *W1* and *W2* magnitudes. Approximately 90 per cent of these have measured 2MASS *JHK* magnitudes. In the control field, there are a total of 18,070 sources with NUV, *W1*, and *W2* magnitudes, and again ~ 90 per cent also have measured 2MASS magnitudes.

2.3 Identification of Candidate Stars

2.3.1 Synthetic Stellar Spectra

We use synthetic stellar spectra to determine colors and apparent magnitudes consistent with OB stars at the distance of the Smith Cloud. The BaSeL 2.2 library (Lejeune et al. 1998) provides synthetic spectra that cover the necessary wavelength range to include all *GALEX*, *WISE*, and 2MASS passbands, and the models range over stellar surface temperatures from 2000 K to 50000 K. We choose stellar models with metallicities of $0.05Z_\odot$ and $0.5Z_\odot$, which bracket the range of possible metallicities of the Smith Cloud ($0.05\text{--}0.4Z_\odot$) constrained by Hill et al. (2009). Model magnitudes are obtained by convolving the synthetic spectra with the filter profiles of all passbands.

2.3.2 Color Cuts

To isolate OB stars, we explore how the BaSeL spectral models are distributed in an NUV–*W1* vs. *W1* – *W2* diagram (Fig. 2). In the synthetic models, all OB stars (defined to have surface temperatures $> 10^4$ K) have NUV–*W1* < 1.8 , which we use as our first cut. We also find that the model stars have *W1*–*W2* ~ 0 , which is consistent with prior studies by Wu et al. (2012) and Yan et al. (2013). These same authors show that quasars become a significant number of point sources at *W1* – *W2* > 0.2 , while Mace et al. (2013) find YSOs at *W1* – *W2* > 0.5 . Thus, to avoid contamination from these point sources while keeping nearly all stars, we keep only objects with *W1* – *W2* < 0.2 . We place no lower limit on the *W1* – *W2* colors of stellar candidates since we find that stars tend to be biased towards bluer colors at dimmer magnitudes (see § 3.1.1). Wherever 2MASS magnitudes are available, we further isolate OB stars by rejecting all sources with $J - H > 0$ and $H - K > 0.02$. These cuts are taken from Straizys & Lazauskaitė (2009), who measured these colors for stars of known spectral type. For all three of our color cuts, we allow a star to pass a color cut if its 1σ uncertainty potentially places it in OB star parameter space, even if its measured value is outside.

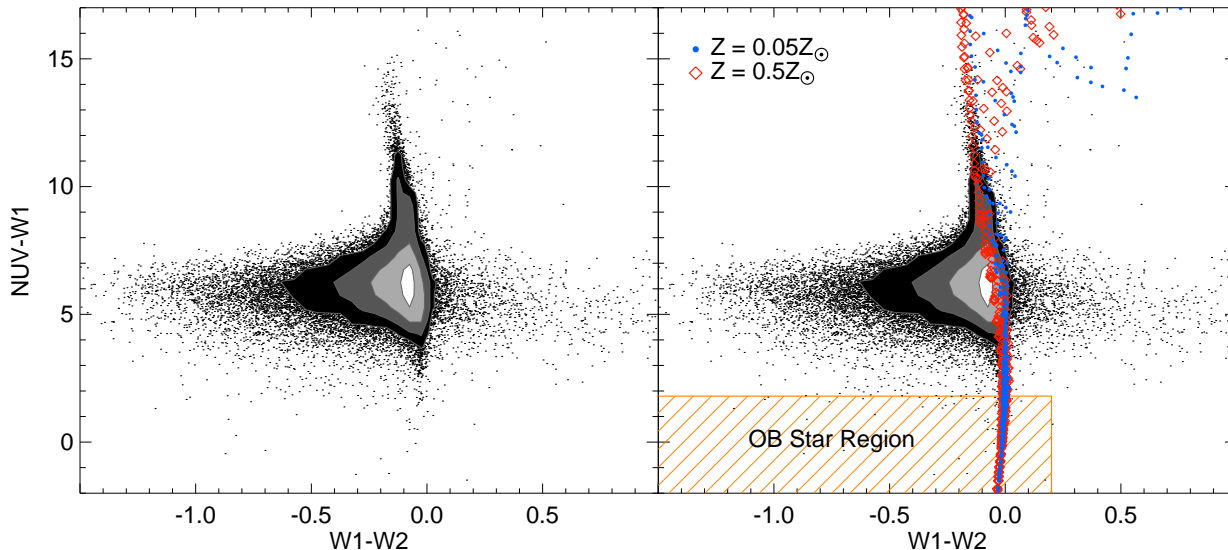


Figure 2. (*left*) Our *GALEX/WISE* crossmatched sources, both on and off the cloud. Filled contours represent regions where the number of stars in a 0.5×0.05 box ($\text{NUV}-W1 \times W1 - W2$) falls above 100, 250, 500, and 1000. (*right*) Model spectral colors (red and blue points) from the BaSeL 2.2 library overlaid on top of the data. The two BaSeL model sets shown, with metallicities of $0.05Z_{\odot}$ and $0.5Z_{\odot}$, approximate the minimum and maximum possible metallicities of the cloud ($0.05Z_{\odot}$ and $0.4Z_{\odot}$; Hill et al. 2009). The hashed region defined by $\text{NUV}-W1 < 1.8$ and $W1 - W2 < 0.2$ shows the expected positions of OB stars free of contamination from QSOs and YSOs. The synthetic colors derived from both models are almost identical in the region of parameter space occupied by OB stars. The scatter in $W1 - W2$ at higher $\text{NUV}-W1$ is real (§ 2.3.1) and does not compromise our analysis.

Fig. 2 shows the model colors overlaid on our data for the Smith Cloud *GALEX* fields (both on and off the cloud). The model colors are consistent with the data, although there is considerable scatter in $W1 - W2$ at $2 < \text{NUV}-W1 < 9$. Such scatter has been seen in other studies (Wu et al. 2012; Yan et al. 2013) and does not affect our analysis, which is restricted to lower values of $\text{NUV}-W1$. The crosshatched area denotes the region of parameter space occupied by OB stars.

2.3.3 Apparent Magnitude Cuts

Since the Smith Cloud has a well constrained distance of 12.4 ± 1.3 kpc (Lockman et al. 2008), we have the advantage of being able to predict the range of possible apparent magnitudes of its OB star population. Expected *NUV*, *W1*, and *J* band absolute magnitudes are estimated using BaSeL spectral models to estimate surface flux while adopting typical stellar radii as a function of spectral type (Habets & Heintze 1981; Massey et al. 2004; Repolust et al. 2004; Massey et al. 2005, 2009). We estimate that between surface temperatures of $1\text{--}5 \times 10^4$ K, OB star luminosities can vary by a factor of $\sim 2 \times 10^4$, ~ 500 , and ~ 700 in the *NUV*, *W1*, and *J* bands respectively. There are additional variations in apparent OB star brightness caused by stars occupying the full width of the cloud along the line of sight, which we estimate to be approximately 325 pc (1.5 degrees), which was measured in the region where we have imaging and assumes the cloud is axisymmetric. Metallicity has a negligible effect on the intrinsic stellar luminosities, causing differences of only ~ 0.03 magnitudes between $0.05Z_{\odot}$ and $0.5Z_{\odot}$, so we use a $0.1Z_{\odot}$ model for our absolute magnitude calculations and ignore any metallicity variations. Lastly,

to account for the uncertainty in the distance to the Smith Cloud, we recalculate the allowed range of apparent OB star brightnesses in steps of 150 pc ($\sim 325/2$) from $12.4\text{--}1.3$ to $12.4+1.3$ kpc. Over the full range of possible distances, the minimum and maximum allowed apparent magnitudes shift by ~ 0.5 mags, but this shift does not have a significant effect on the final results (see § 3.1.1). The accepted ranges of apparent magnitudes for OB stars in the Smith Cloud are given in Table 2. As with our color cuts, we allow a star to pass a brightness cut if its uncertainty potentially places it within the range of brightnesses occupied by OB stars.

At this point, we can revisit the 45 per cent of *NUV* sources that are not detected by *WISE*. Most of these objects have *NUV* magnitudes of 23–23.5, and to be undetected by *WISE* they must have $W1 \gtrsim 17$, the 5σ sensitivity of the survey. Our model apparent magnitudes show that objects this dim are inconsistent with OB stars at the distance of the Smith Cloud. Thus, we are at no risk of missing any candidates by ignoring these sources. Additionally, our model magnitudes show that shallow *GALEX* AIS imaging is capable of detecting young OB stars at the distance of the Smith Cloud. The dimmest OB star we include has $m_{\text{NUV}} = 18.2$, corresponding to $m_{\text{NUV}} = 20.2$ after adding in the typical foreground extinction of ~ 2 magnitudes. Thus, the dimmest OB star before extinction corrections is still brighter than the AIS completeness limit of 20.5 magnitudes.

3 RESULTS

3.1 Number of Candidate OB Stars

All sources in the Smith Cloud and the control fields are passed through our calibrated color and apparent magnitude

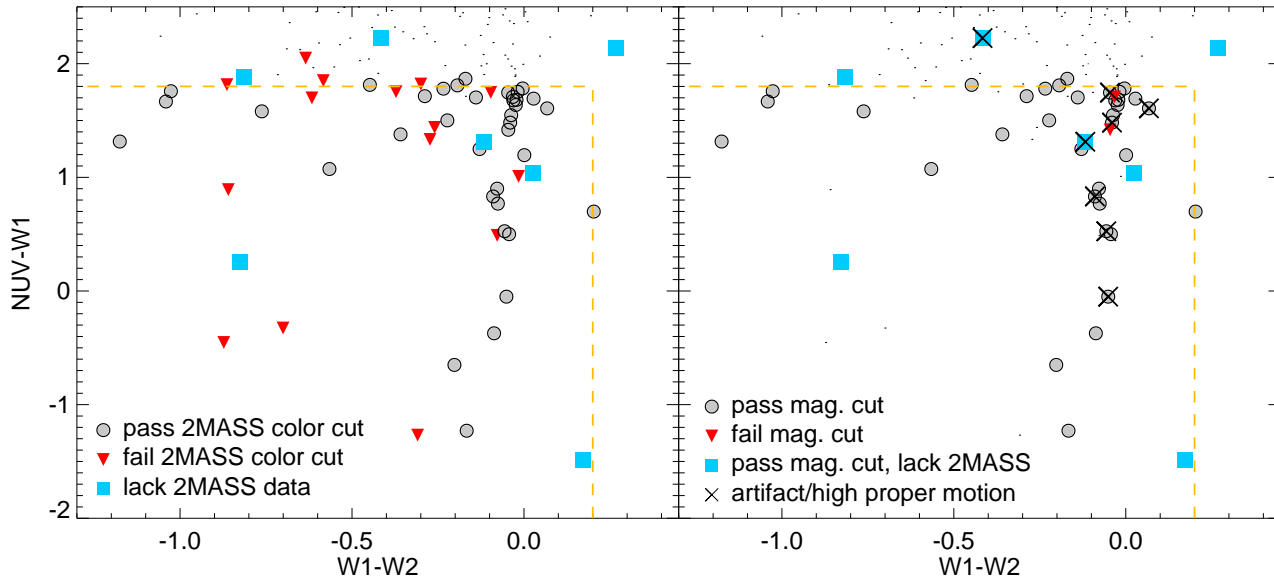


Figure 3. Zoomed in version of Fig. 2 showing the results of the color and magnitude cuts. The region within the orange dashed line is identical to the hashed region in Fig. 2. (*left*) Results of the color cuts described in § 2.3.2. All large points inside passed the $NUV-W1$ and $W1-W2$ color cuts. Points lying outside the parameter space of OB stars can still pass the color cuts if their 1σ uncertainties potentially place them within the OB star region. Filled grey points represent stars that also passed the $J-H$ and $H-K$ cuts using 2MASS data. Red triangles represent stars that failed the $J-H$ and $H-K$ cuts. Blue filled squares represent stars that but lacked 2MASS data. The grey and blue points are kept and passed through the magnitude cuts. (*right*) Results of the magnitude cuts described in § 2.3.3. Stars that failed the previous color cuts are shown as small black dots. Filled grey points represent stars that passed the NUV , $W1$, and J band magnitude cuts assuming the Smith Cloud is at a distance of 12.4 kpc. Red triangles represent stars that failed the magnitude cuts in at least one band. Blue points represent stars that passed the NUV and $W1$ magnitude cuts but lacked 2MASS data. The X’s denote stars that were cut due to having high proper motions or were potentially affected by *GALEX* NUV image artifacts. The 34 grey and blue points without X’s make up our final sample of candidate OB stars shown in Fig. 5.

Table 2. Apparent Magnitude Limiting Values

Band	Minimum	Maximum
<i>GALEX</i> NUV	8.1(7.8,8.3)	18.2(17.9,18.4)
<i>WISE</i> W1	10.7(10.5,11.0)	16.8(16.5,17.0)
2MASS <i>J</i>	10.5(10.2,10.7)	16.8(16.5,17.0)

Apparent magnitudes assume a distance of 12.4 kpc and minimum/maximum values reflect expected variation due to the intrinsic range of OB star luminosities and the thickness of the Smith Cloud. Values in parentheses give the expected range of magnitudes at the closest (11.1 kpc) and furthest (13.7 kpc) possible Smith Cloud distances based on the error bars from the existing distance estimate of Lockman et al. (2008). *GALEX* magnitudes are given in the AB system, while *WISE* and 2MASS magnitudes are given in the Vega system.

cuts to identify stars that may plausibly be OB stars at the distance of the Smith Cloud. Here we describe the results.

3.1.1 Smith Cloud Field

After applying $W1-W2$, $NUV-W1$, $J-H$, and $H-K$ color cuts, we are left with 44 candidate OB stars in the Smith Cloud field, seven of which lack 2MASS magnitudes (Fig. 3). Assuming the nominal distance of the Smith Cloud, the apparent magnitude cuts reject two stars. As described in § 2.3.3, to see how the results depend on the uncertainty in the distance to the cloud, we rerun the magnitude cuts

in steps from 11.1 kpc to 13.7 kpc. Across the full range of distances, the total number of stars rejected by the magnitude cuts remains roughly constant at two stars, but up to 3–4 stars are rejected close to the nearest and furthest allowed distances. Thus, after the magnitude cut, we are left with 40–42 candidate OB stars, depending on the assumed distance to the Smith Cloud.

We then searched the SIMBAD stellar database to see if any of the remaining stars had measured proper motions. We used these proper motions to calculate lower limits on their true space velocities assuming the stars are at the distance of the Smith Cloud, and then compared these velocities to the true motion of the Smith Cloud through space, which is estimated to be $\sim 300 \text{ km s}^{-1}$ (Lockman et al. 2008). Of the candidate stars, four have cataloged proper motions, three of which yield velocities $\sim 1000 \text{ km s}^{-1}$ or larger, which we judge to be unrealistically high and reject. The remaining star has a velocity $> 70 \text{ km s}^{-1}$. We deem this to be plausibly associated with the Smith Cloud and keep it in the list of OB star candidates.

After accounting for measured proper motions, we examined all artifact flags in the *GALEX* catalog, and an additional five stars were rejected due to their fluxes being potentially corrupted by NUV artifacts. The combination of rejecting stars with high proper motions and those potentially affected by NUV artifacts serendipitously removes any dependence of our final result on the distance to the cloud. As described above, the magnitude cuts reject slightly different numbers of stars depending on the assumed distance.

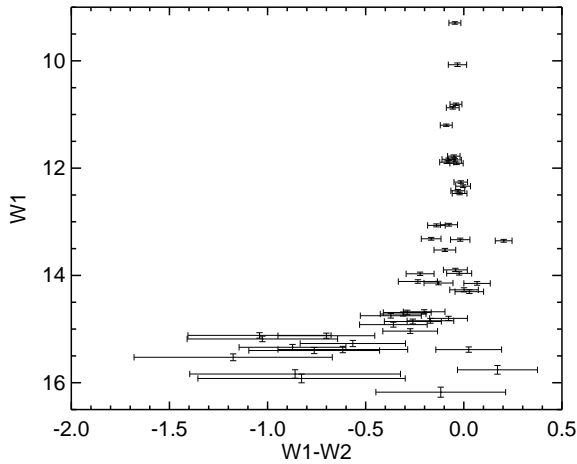


Figure 4. $W1$ vs. $W1 - W2$ for all stars in the Smith Cloud field with $\text{NUV}-W1 < 1.8$. At dimmer magnitudes, colors tend to be biased towards bluer values in conjunction with larger photometric uncertainties.

Of the stars that were rejected at some distances but not others, all of them either had high proper motion or were affected by NUV artifacts, so ended up being rejected regardless of their apparent magnitudes. In summary, we are left with a total of 34 candidate OB stars found in the Smith Cloud field, 21 of which fall directly on the cloud.

Several of our final candidate OB stars lie at much bluer $W1 - W2$ colors than expected for main sequence stars (which typically have $W1 - W2 \sim 0$; see § 2.3.2). Fig. 4 shows a *WISE* color-magnitude diagram for all stars with $\text{NUV}-W1 < 1.8$. Stars at dimmer magnitudes tend to be biased towards bluer colors. Thus, we consider objects with such blue $W1 - W2$ colors as valid OB star candidates, and attribute their unusual colors to large photometric uncertainties.

3.1.2 Control Field

In the control field, the *GALEX*, *WISE*, and 2MASS color cuts leave 11 candidate stars, all of which have 2MASS magnitudes. All of these stars pass the apparent magnitude cuts over the entire range of possible distances to the Smith Cloud. An additional two stars are removed for having large proper motions, and three more stars are removed due to potential contamination from NUV artifacts. This selection leaves six candidate OB stars in the control field.

3.2 Likelihood of Association

The numbers of stars and projected space densities in each region are presented in Table 3. The uncertainties in Table 3 are computed using Poisson statistics so that the uncertainty of each measurement of N stars is \sqrt{N} . As discussed before, there does not appear to be any additional uncertainty introduced due to the uncertainty in the distance to the Smith Cloud or its metallicity.

The 34 final candidate OB stars in the Smith Cloud field are overlaid on the HI column density map in Fig. 5 and the

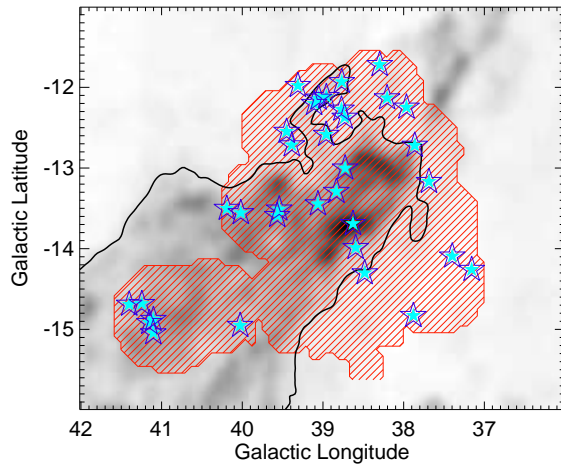


Figure 5. The final 34 candidate OB stars (blue) overlaid on the Smith Cloud HI column density map. The red filled region indicates the spatial extent of our *GALEX* data, while the solid black line indicates the $5 \times 10^{19} \text{ cm}^{-2}$ contour used to define the edge of the cloud.

Table 3. OB Star Candidates in Different Regions

Region	N	Area (kpc^2)	Density (kpc^{-2})
On Cloud	21 ± 4.6	0.28	75.0 ± 16.4
Off Cloud	13 ± 3.6	0.23	56.5 ± 15.7
On+Off Cloud	35 ± 5.9	0.51	68.6 ± 11.5
Control	6 ± 2.4	0.16	37.5 ± 15.0
On Cloud – Control	11 ± 6.2	0.28	39.3 ± 22.1
Leo P	7 ± 2.7	0.39	17.9 ± 6.9

We adopt a distance of 12.4 kpc (Lockman et al. 2008) to calculate the physical area of all regions except Leo P, for which we adopt a distance of 1.75 Mpc (Giovanelli et al. 2013).

surface densities of OB candidate stars in each region are compared in Fig. 6. Stars are preferentially found in the region we have defined to be ‘on’ the cloud, but the number of stars found ‘on’ versus ‘off’ the cloud are the same within their uncertainties. Several stars are positioned very close to the cloud border, so that increasing the limiting column density by only 0.1 dex would cause six more stars to fall in the ‘off’ region, making the density of stars ‘off’ the cloud larger than ‘on’, although these numbers are still consistent within their uncertainties (lighter points in Fig. 6).

Instead of separating the Smith Cloud field into regions ‘on’ and ‘off’ the cloud, we could justifiably consider the possibility that all stars in this region are associated with the Smith Cloud. This assumption is reasonable considering stars can drift away from their birth clouds over the course of their lifetimes. Observations of young clusters show typical radial velocity dispersions of $\sim 20 \text{ km s}^{-1}$ (see, e.g., the study of the Perseus OB2 association by Steenbrugge et al. 2003). Multiplying this by the typical age of a B star ($\sim 100 \text{ Myr}$), drift distances of up to 2 kpc are possible over OB star lifetimes, equivalent to 9.4 degrees at the distance of the Smith Cloud. This angular radius encompasses > 16 times the area of all our *GALEX* coverage on the Smith Cloud.

Regardless of whether we assume all stars in our *GALEX* fields are associated with the cloud, or only those within the $N_{\text{HI}} = 5 \times 10^{19} \text{ cm}^{-2}$ contour, the spatial density of stars is higher than the density of stars in the control field, but not at a statistically significant level (Fig. 6).

4 DISCUSSION

4.1 Comparison to Theoretical Expectations

It is instructive to ask how many OB stars we might actually expect to form in an object such as the Smith Cloud. To address this question, we measure the typical gas surface density in the cloud and use it to infer the range of possible star formation rate surface densities. In regions within the outermost $N_{\text{HI}} = 5 \times 10^{19} \text{ cm}^{-2}$ contour and overlapping our search fields, the median column density is $1.5 \times 10^{20} \text{ cm}^{-2}$ or $1.2 M_{\odot} \text{ pc}^{-2}$ (not corrected for Helium). Bigiel et al. (2010) examined the relationship between star formation rate and HI surface density (also without Helium corrections) on sub-kpc scales in the outer disks of dwarf galaxies, and found that 75 per cent of regions at comparable gas density form stars at rates between approximately $10^{-(4.2-5.2)} M_{\odot} \text{ yr}^{-1} \text{ kpc}^{-2}$. We use this range of star formation rates to calculate the number of OB stars at masses greater than $2.15 M_{\odot}$ (corresponding to stars $> 10^4 \text{ K}$ according to the same tabulations of stellar properties referenced in § 2.3.3) expected under two scenarios: (1) one where the Smith Cloud has been forming stars continuously for 10 Gyr, and (2) another where the Smith Cloud has been forming stars only since its first impact with the Milky Way 70 Myr ago (Lockman et al. 2008; Nichols & Bland-Hawthorn 2009). In both cases, we assume that the star formation follows a Salpeter IMF, that the star formation rate and average HI surface density have remained constant, and that stellar ages can be approximated by $\tau_{\text{MS}} = 10^{10} (M/M_{\odot})^{-2.5} \text{ yr}$.

Under the 10 Gyr scenario, we expect between 45 and 390 OB stars on the ‘ON’ field of the Smith Cloud (or $\sim 160\text{--}1380 \text{ kpc}^{-2}$), far more than we observe. Under the 70 Myr scenario, we would expect to find between 5 and 40 OB stars (or $\sim 18\text{--}140 \text{ kpc}^{-2}$) in this same region, which is consistent with the observations. The grey region in Fig. 6 shows the range of OB star densities we would expect to measure in the 70 Myr scenario. Unfortunately, this range does not allow us to reject or confirm the Smith Cloud as a star forming cloud because all the regions considered, including the control field, are consistent with this star formation scenario.

For comparison, instead of calculating the expected number of OB stars based on the star formation rate estimated using gas density, we can reverse the calculation to estimate what star formation rate would yield our observed number of stars, again assuming constant star formation over either the last 10 Gyr or 70 Myr and that the star formation follows a Salpeter IMF. First, we assume all 21 candidate OB stars on the cloud are indeed associated with the cloud. To recreate our observations under the 10 Gyr scenario would require a star formation rate surface density of $10^{-5.5 \pm 0.1} M_{\odot} \text{ yr}^{-1} \text{ kpc}^{-2}$. Under the 70 Myr scenario, a star formation rate surface density of $10^{-4.5 \pm 0.1} M_{\odot} \text{ yr}^{-1} \text{ kpc}^{-2}$ would create the observed number of stars. Alternatively, if we proceed with the assumption

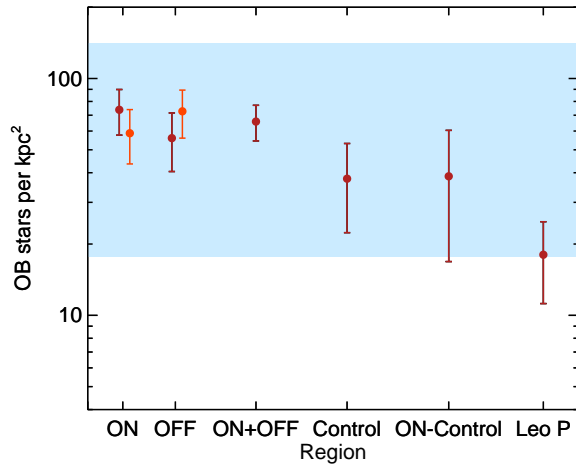


Figure 6. The measured density of candidate OB stars in different regions of this study. The blue band represents the range in surface density of OB stars given the range in possible star formation rates based on the typical gas density of the cloud, and assuming star formation began 70 Myr ago when the cloud first passed through the Galactic disk. The lighter points immediately to the right of the ‘ON’ and ‘OFF’ points represent the values if the HI column density used to define the edge of the cloud is increased by 0.1 dex.

that the OB star density measured in the control field is a good measure of the background from the Milky Way, then 10 out of the 17 observed stars are actually associated with the Smith Cloud. This implies star formation rate surface densities of $10^{-5.8 \pm 0.3} \text{ yr}^{-1} \text{ kpc}^{-2}$ and $10^{-4.8 \pm 0.3} \text{ yr}^{-1} \text{ kpc}^{-2}$ for the 10 Gyr and 70 Myr scenarios respectively. Whether we subtract a background OB star density or not, the 70 Myr scenario is the only one consistent with the expected range of star formation rates based on gas surface density from Bigiel et al. (2010), and is likely a better description of the cloud’s star formation history.

4.2 Comparison with Leo P

The newly discovered galaxy Leo P was originally identified as a UCHVC within the ALFALFA survey (Giovannelli et al. 2010). Follow-up observations by McQuinn et al. (2013) and Rhode et al. (2013) revealed the clear presence of a stellar population and ongoing star formation, making it the best existing example of an ‘HVC turned galaxy’. Since we are trying to determine whether the Smith Cloud is a similar object, it is instructive to compare its properties with Leo P.

Despite its original designation as a UCHVC, Leo P is not dramatically smaller than the Smith Cloud. HI observations with the JVLA and Arecibo reveal that it is approximately 1/3 the size of the Smith Cloud and has almost an equivalent HI mass (Giovannelli et al. 2013). However, given the Smith Cloud’s recent history of interaction with the Milky Way, its original HI mass may have been much larger (~ 10 times greater according to Nichols & Bland-Hawthorn 2009), and it has an ionized gas component equal to or greater than its neutral component (Hill et al. 2009). The ionized gas fraction of Leo P is unconstrained. The peak HI

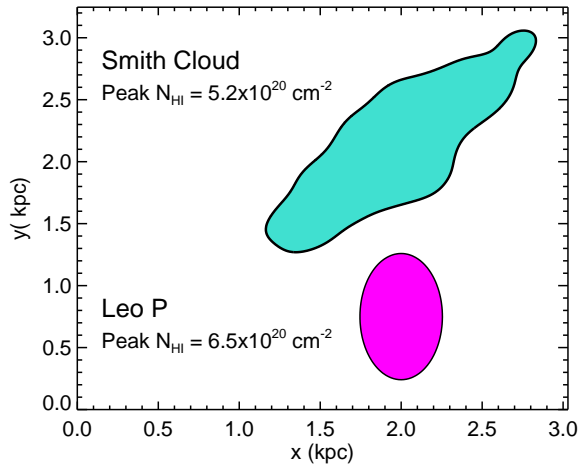


Figure 7. Leo P’s size relative to that of the Smith Cloud if both were placed at the same distance. Outlines represent the $5 \times 10^{19} \text{ cm}^{-2}$ contours. The Smith Cloud outline is based on an HI map convolved to 200 pc resolution. The Leo P shape is an approximation based on the published radius and axis ratio from Giovanelli et al. (2013). Peak column densities come from Lockman et al. (2008) and Bernstein-Cooper et al. (2014).

column densities of the Smith Cloud and Leo P are very comparable. At an equivalent spatial resolution of ~ 30 pc, both show comparable peak column densities around $\sim 5 \times 10^{20} \text{ cm}^{-2}$ (Lockman et al. 2008; Bernstein-Cooper et al. 2014). Leo P has a gas phase metallicity of $\sim 3\% Z_{\odot}$ (Skillman et al. 2013), consistent with (or possibly even lower than) that of the Smith Cloud.

Deep V and I band imaging of Leo P was presented in McQuinn et al. (2013). We use the $V - I$ color-temperature relation of Worthey & Lee (2011) to isolate OB stars with surface temperatures $> 10^4$ K, or $V - I < 0.036$. Using this color cut, we find a total of 7 OB stars in Leo P. Like we did for the Smith Cloud, if we use the approximate area within the $5 \times 10^{19} \text{ cm}^{-2}$ contour (which contains all the identified OB stars, although the photometric data extend to larger radius), we obtain an OB star density less than that found in the direction of the Smith Cloud (see Fig. 6, Table 3). Therefore, if Leo P were placed at the position of the Smith Cloud, its OB star population would not be detected to a statistically significant level by our analysis. This result implies that star formation within the Smith Cloud may be present but simply undetected due to Milky Way contamination.

5 CONCLUSIONS

Using a combination of 21cm, NIR, and UV data, we conducted a search for young stars potentially associated with the Smith Cloud, an HVC currently on a collision course with the Milky Way. Using a combination of color and apparent magnitude cuts, we identified 34 candidate OB stars out of $\sim 40,000$ sources in a field overlapping the Smith cloud, with 21 of these stars falling directly over the cloud, although this number is sensitive to the specific definition of the cloud edge. Regardless, the number density of candidate stars in

the Smith Cloud field is slightly higher than the density of a control region, but not at a statistically significant level.

We have compared the number of candidate OB stars to theoretical expectations based on the gas density of the cloud. We find that the number of candidate stars is consistent with a scenario where constant star formation began 70 Myr ago when the cloud first impacted the Galactic disk, but is not consistent with a scenario where the cloud has been constantly forming stars over the last several Gyr. We estimate the star formation rate surface density of the cloud to be $10^{-4.8 \pm 0.3} M_{\odot} \text{ yr}^{-1} \text{ kpc}^{-2}$, again assuming constant star formation triggered ~ 70 Myr ago.

Lastly, we have compared the properties of the Smith Cloud with those of the recently discovered star forming galaxy that was originally classified as a UCHVC, Leo P. We find that these two objects have comparable HI properties (mass, size, peak column density) and gas-phase metallicities. Leo P, although hosting a stellar population and ongoing star formation, would not be detectable via our method if it were placed at the position of the Smith Cloud. This means that if the Smith Cloud is forming stars, it may be doing so at a low rate comparable to dwarf galaxies like Leo P and yet be indiscernible from the Milky Way foreground using our photometric techniques alone.

On the other hand, if the Smith Cloud is not forming stars, this raises the question of how it is different from Leo P. Both objects show comparable maximum column densities, but Leo P’s column density may translate into a higher *volume* density since the gas is confined to a disk, whereas the Smith Cloud has an unknown thickness along the line of sight. Any lack of star formation in the Smith Cloud would be unlikely to be due to metallicity considering that Leo P’s metallicity is comparable to the Smith Cloud’s. A final major consideration is the difference in dynamical properties of these systems. The Smith Cloud is undergoing a major interaction with the Milky Way. While the tidal forces or cloud collisions involved in this interaction could promote star formation (initially, we thought this interaction might raise the likelihood of seeing star formation), the cloud’s disruption may impart enough additional turbulence to help support against collapse, all while gas is continuously being removed via stripping by the corona (Heitsch & Putman 2009). Meanwhile, Leo P is relatively isolated with no known object within 0.5 Mpc (McQuinn et al. 2013). However, any effect attributed to these differences is at this point speculative, as our data are consistent with the possibility that the Smith Cloud does host star formation.

Our results leave open the possibility that the Smith Cloud is a galaxy yet waiting to be discovered. Unfortunately, its position with respect to the Milky Way and its vast extent make studying it challenging. Spectroscopy of the stars at the position of the Smith Cloud, to identify distinct kinematics or metallicities, is a potentially promising path to determine whether it hosts its own stellar population.

ACKNOWLEDGMENTS

We thank the referee for their helpful comments that improved this paper. We also thank Jay Lockman for sharing his HI data cube for the Smith Cloud and instructing us on

its use, as well as for his helpful comments for this study. We also thank Fabian Heitsch for his valuable input on the *GALEX* proposal from which we obtained our data and the overall study. We also thank Alex Hill and Mary Putman for useful discussions and suggestions. This program was funded by the *GALEX* Guest Investigator program under NASA grant NNX10AR88G. This publication makes use of data products from the Wide-field Infrared Survey Explorer, which is a joint project of the University of California, Los Angeles, and the Jet Propulsion Laboratory/California Institute of Technology, funded by the National Aeronautics and Space Administration. This publication makes use of data products from the Two Micron All Sky Survey, which is a joint project of the University of Massachusetts and the Infrared Processing and Analysis Center/California Institute of Technology, funded by the National Aeronautics and Space Administration and the National Science Foundation. This research has made use of the SIMBAD database, operated at CDS, Strasbourg, France.

REFERENCES

- Adams E. A. K., Giovanelli R., Haynes M. P., 2013, *ApJ*, 768, 77
- Bernstein-Cooper E. Z. et al., 2014, *AJ*, 148, 35
- Bigiel F., Leroy A., Walter F., Blitz L., Brinks E., de Blok W. J. G., Madore B., 2010, *AJ*, 140, 1194
- Bigiel F., Leroy A., Walter F., Brinks E., de Blok W. J. G., Madore B., Thornley M. D., 2008, *AJ*, 136, 2846
- Bland-Hawthorn J., Veilleux S., Cecil G. N., Putman M. E., Gibson B. K., Maloney P. R., 1998, *MNRAS*, 299, 611
- Blitz L., Spergel D. N., Teuben P. J., Hartmann D., Burton W. B., 1999, *ApJ*, 514, 818
- Braun R., Burton W. B., 1999, *A&A*, 341, 437
- Casetti-Dinescu D. I., Moni Bidin C., Girard T. M., Méndez R. A., Vieira K., Korchagin V. I., van Altena W. F., 2014, *ApJ*, 784, L37
- Christodoulou D. M., Tohline J. E., Keenan F. P., 1997, *ApJ*, 486, 810
- de Blok W. J. G., Walter F., 2006, *AJ*, 131, 363
- Giovanelli R. et al., 2013, *AJ*, 146, 15
- Giovanelli R., Haynes M. P., Kent B. R., Adams E. A. K., 2010, *ApJ*, 708, L22
- Gould R. J., Salpeter E. E., 1963, *ApJ*, 138, 393
- Habets G. M. H. J., Heintze J. R. W., 1981, *A&AS*, 46, 193
- Heitsch F., Putman M. E., 2009, *ApJ*, 698, 1485
- Hernandez A. K., Wakker B. P., Benjamin R. A., French D., Kerp J., Lockman F. J., O’Toole S., Winkel B., 2013, *ApJ*, 777, 19
- Hill A. S., Haffner L. M., Reynolds R. J., 2009, *ApJ*, 703, 1832
- Hill A. S., Mao S. A., Benjamin R. A., Lockman F. J., McClure-Griffiths N. M., 2013, *ApJ*, 777, 55
- Hopp U., Schulte-Ladbeck R. E., Kerp J., 2003, *MNRAS*, 339, 33
- Hopp U., Schulte-Ladbeck R. E., Kerp J., 2007, *MNRAS*, 374, 1164
- Ivezic Z., Christodoulou D. M., 1997, *ApJ*, 486, 818
- Joung M. R., Bryan G. L., Putman M. E., 2012, *ApJ*, 745, 148
- Klypin A., Kravtsov A. V., Valenzuela O., Prada F., 1999, *ApJ*, 522, 82
- Lejeune T., Cuisinier F., Buser R., 1998, *VizieR Online Data Catalog*, 413, 65
- Lockman F. J., Benjamin R. A., Heroux A. J., Langston G. I., 2008, *ApJ*, 679, L21
- Mac Low M.-M., Glover S. C. O., 2012, *ApJ*, 746, 135
- Mace G. N. et al., 2013, *ApJS*, 205, 6
- Massey P., Bresolin F., Kudritzki R. P., Puls J., Pauldrach A. W. A., 2004, *ApJ*, 608, 1001
- Massey P., Puls J., Pauldrach A. W. A., Bresolin F., Kudritzki R. P., Simon T., 2005, *ApJ*, 627, 477
- Massey P., Zangari A. M., Morrell N. I., Puls J., DeGioia-Eastwood K., Bresolin F., Kudritzki R.-P., 2009, *ApJ*, 692, 618
- McQuinn K. B. W. et al., 2013, *AJ*, 146, 145
- Morrissey P. et al., 2007, *ApJS*, 173, 682
- Nichols M., Bland-Hawthorn J., 2009, *ApJ*, 707, 1642
- Nichols M., Mirabal N., Agertz O., Lockman F. J., Bland-Hawthorn J., 2014, *ArXiv e-prints*
- O’Donnell J. E., 1994, *ApJ*, 422, 158
- Putman M. E., Bland-Hawthorn J., Veilleux S., Gibson B. K., Freeman K. C., Maloney P. R., 2003, *ApJ*, 597, 948
- Putman M. E., Peek J. E. G., Joung M. R., 2012, *ARA&A*, 50, 491
- Repolust T., Puls J., Herrero A., 2004, *A&A*, 415, 349
- Rhode K. L. et al., 2013, *AJ*, 145, 149
- Richter P., Sembach K. R., Wakker B. P., Savage B. D., 2001, *ApJ*, 562, L181
- Schlegel D. J., Finkbeiner D. P., Davis M., 1998, *ApJ*, 500, 525
- Sembach K. R., Howk J. C., Savage B. D., Shull J. M., 2001, *AJ*, 121, 992
- Siegel M. H., Majewski S. R., Gallart C., Sohn S. T., Kunkel W. E., Braun R., 2005, *ApJ*, 623, 181
- Simon J. D., Blitz L., 2002, *ApJ*, 574, 726
- Skillman E. D. et al., 2013, *AJ*, 146, 3
- Smith G. P., 1963, *Bull. Astron. Inst. Netherlands*, 17, 203
- Steenbrugge K. C., de Bruijne J. H. J., Hoogerwerf R., de Zeeuw P. T., 2003, *A&A*, 402, 587
- Sternberg A., McKee C. F., Wolfire M. G., 2002, *ApJS*, 143, 419
- Straižys V., Lazauskaitė R., 2009, *Baltic Astronomy*, 18, 19
- Thilker D. A. et al., 2007, *ApJS*, 173, 538
- Wakker B. P., van Woerden H., 1997, *ARA&A*, 35, 217
- Wakker B. P., York D. G., Wilhelm R., Barentine J. C., Richter P., Beers T. C., Ivezić Ž., Howk J. C., 2008, *ApJ*, 672, 298
- Willman B., Dalcanton J., Ivezić Ž., Schneider D. P., York D. G., 2002, *AJ*, 124, 2600
- Worthey G., Lee H.-c., 2011, *ApJS*, 193, 1
- Wright E. L. et al., 2010, *AJ*, 140, 1868
- Wu X.-B., Hao G., Jia Z., Zhang Y., Peng N., 2012, *AJ*, 144, 49
- Yan L. et al., 2013, *AJ*, 145, 55